Rest-to-Rest Motion of an Experimental Flexible Structure Subject to Friction: Linear Programming Approach

Rajaey Kased
e-mail: kased@eng.buffalo.edu

Tarunraj Singh[1]
e-mail: tsingh@buffalo.edu

Department of Mechanical and Aerospace Engineering,
University at Buffalo,
Buffalo, NY 14260

A linear programming approach designed to eliminate the residual vibration of the two-mass harmonic system subject to friction and undergoing a point-to-point maneuver is proposed and implemented on an experimental test bed. Techniques for design of positive pulse control profiles for nonrobust and robust open loop controller design are explored, where the positive pulses initiate motion and the friction force brings the system to rest. It is shown that consistent results can be obtained from experiments and the robustness against frequency uncertainty results in the reduction in residual vibration as well as steady-state error. [DOI: 10.1115/1.4000460]

1 Introduction

Linear programming (LP) is a powerful numerical optimization technique that is able to handle hundreds of constraints efficiently. It requires all the constraints and the cost to be linear in the unknown variables. This restriction on the use of LP may seem to preclude its use on real engineering problem. It is possible, however, to formulate some complex nonlinear control problems to fit the required form of LP [1] as illustrated in Ref. [2], where a nonlinear constraint representing fuel usage is rewritten as two linear constraints.

LP has been used to design time-optimal and fuel limited time-optimal control for linear systems [3,4,2], where magnitude constraints on the discrete input sequence $u(k)$ are imposed to result in a bang-bang or bang-off-bang control profile. Since posing the problem in a LP framework requires a discrete time representation of the system, the resulting control profile tends to the optimal control profile as the number of samples over the duration of the maneuver increases. If the exact time-optimal or fuel limited time-optimal control profile is desired, the solution of the LP problem can be used to parameterize the control profile in continuous time [5,6] using the switch times as variables. The number of switches can be determined from the solution of the LP problem.

Friction plays an important role in the point-to-point maneuvering class of problems. Positioning applications include telescopes, antennas, machine tools, disk drives, robots etc. Velocity control is also relevant in industrial applications such as machine tool, disk drive, and robot arm control, which require the accurate tracking of a predetermined trajectory. The effect of friction becomes accentuated in the low velocity regions near the reference position, which influences the steady-state behavior of the control system.

The majority of work done on the control of frictional systems is on rigid body systems. Yang and Tomizuka [7] exploited a simple relationship between a pulse input and the displacement of the rigid body to design a control technique where the pulse initiates the motion and the friction mechanism dissipates the energy in the system, bringing it to rest. This utilizes the fact that the rigid body subject to a pulse input never changes the sign of its velocity and thus the Coulomb friction acts as a bias input. This scheme, known as pulse width control (PWC), is presented in an adaptive control setting, where an estimate of the friction is determined in real-time and is subsequently used to design a pulse to eliminate the tracking error. Repeated application of the PWC resulted in very precise tracking. van de Wijdeven and Singh [8] modified the PWC approach to increase the accuracy in a discrete time implementation of the input. Their technique modulates the pulse height to compensate for the inability of a discrete time control profile to accurately reproduce a pulse width designed without accounting for the constraints on the switch times. They referred to their technique as pulse amplitude pulse width control (PAPWC).

Additional schemes developed for rigid body systems include internal-model following error control [9], proportional integral derivative (PID) and state feedback linearization control [10], and variable structure control in order to try to handle qualitatively different friction regimes [11,12]. Nonlinear PID control has also been developed to overcome the stick-slip behavior of friction [13].

Overcoming friction in flexible systems has been sparingly studied. This is despite the fact that the practical use of controllers in this area includes high precision overhead robot arms subject to friction at the joints, high-density hard-disk drives requiring the modeling of the flexibility of the read-write arm, as well as the pivot friction, where the friction effect is noticeable near the reference point.

Rathbun et al. [14] used the PWC control developed for the rigid body directly on the flexible system while ensuring stability by bounding the control gain. The system will, however, result in undesired vibration near the reference point. Hamamoto et al. [15] used iterative feedback tuning to try to control the two-mass harmonic system under the influence of friction. Two controllers (feedback and feedforward) are designed in order to account for the friction and reduce steady-state vibration.

A more recent approach poses the problem in a mixed integer linear programming setting in order to accommodate for the friction sign change for the two-mass harmonic system [16]. Since this is computationally expensive, it precludes fine discretization of the maneuver time. Lawrence et al. [17] used proportional derivative (PD) control on a second order system and input-shapers to try to compensate for the Coulomb friction and eliminate vibration with positive velocity assumption.

The contribution of this paper is the experimental verification of the technique developed by Kim and Singh [18] to eliminate the residual vibration of flexible structures subject to friction, undergoing point-to-point maneuvers. The proposed technique is illustrated on systems where the control input and frictional forces

[1]Corresponding author.

Contributed by the Technical Committee on Vibration and Sound of ASME for publication in the JOURNAL OF VIBRATION AND ACOUSTICS. Manuscript received March 17, 2008; final manuscript received July 30, 2009; published online January 8, 2010. Editor: Kon-Well Wang.

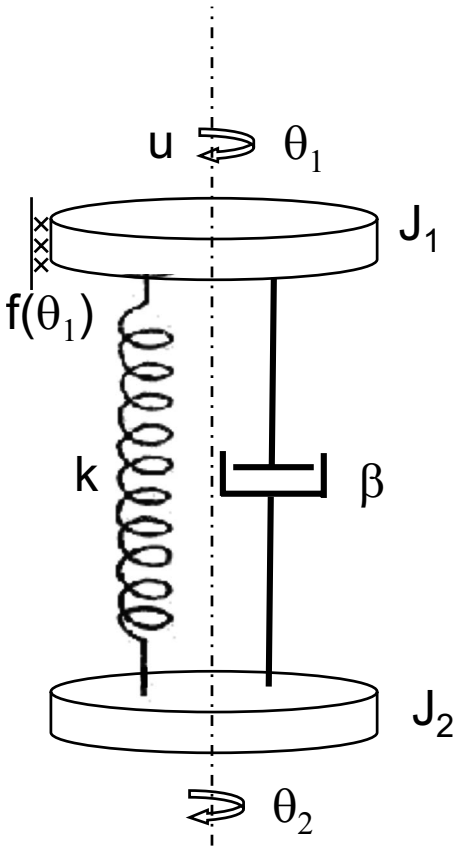

Fig. 1 Two-mass harmonic oscillator

are collocated on an inertia. This approach uses linear programming to solve for optimal control profiles, which satisfy constraints that represent the dynamics of the system as well as positive velocity constraints. Although the accuracy of the control profile is limited by the number of samples and convergence tolerances, linear programming guarantees generation of a near globally optimal control profile. The proposed technique is for small point-to-point displacement in the vicinity of the final position. Any traditional feedback control techniques can be used to get to the proximity of the desired position. Since the goal of the proposed controller is to perform rest-to-rest maneuvers, a simple measure to gauge the performance of the controller is the residual energy, which is the sum of the kinetic energy of the masses and the potential energy of the springs. The larger the deviation of the residual energy from zero, the worse the performance of the controller becomes.

Following the introduction to the problem, the linear programming formulation of the problem is described in Sec. 2. Techniques to include the sensitivity of the system states to uncertainties in the spring stiffness are used to arrive at an augmented system model, the solution of which results in a robust control profile. Section 3 describes the experimental setup and discusses the performance of the proposed controller over multiple runs. The paper concludes with some remarks in Sec. 4.

2 Mathematical Formulation

The flexible structure that is used in this research is the two-mass harmonic oscillator subject to friction, as shown in Fig. 1. The spring and dashpot act at the center of the two disks and are located off-center in Fig. 1 for illustrative purposes only. The equation of motion is

$$\begin{bmatrix} J_1 & 0 \\ 0 & J_2 \end{bmatrix}\begin{bmatrix} \ddot{\theta}_1 \\ \ddot{\theta}_2 \end{bmatrix} + \begin{bmatrix} \beta & -\beta \\ -\beta & \beta \end{bmatrix}\begin{bmatrix} \dot{\theta}_1 \\ \dot{\theta}_2 \end{bmatrix} + \begin{bmatrix} k & -k \\ -k & k \end{bmatrix}\begin{bmatrix} \theta_1 \\ \theta_2 \end{bmatrix} = \begin{bmatrix} 1 \\ 0 \end{bmatrix}(u(t) - f(\dot{\theta}_1)) \tag{1}$$

where J_1 and J_2 are the inertias of the two disks, and β and k are the coefficients of damping and torsional spring stiffness, respectively. The first inertia is in contact with the ground and is subject to a frictional force. θ_1 and θ_2 represent the rotary displacements of the two inertias. The friction model $f(\dot{\theta}_1)$ is the classical static-Coulomb friction model

$$f(\dot{\theta}_1) = \begin{cases} f_c \operatorname{sign}(\dot{\theta}_1), & \text{if } \dot{\theta}_1 \neq 0 \\ f_s \operatorname{sign}(u_{\text{sum}}), & \text{if } \dot{\theta}_1 = 0 \text{ and } u_{\text{sum}} > f_s \\ u_{\text{sum}}, & \text{if } \dot{\theta}_1 = 0 \text{ and } u_{\text{sum}} \leq f_s \end{cases} \tag{2}$$

where u_{sum} is defined as

$$u_{\text{sum}} = u - k(\theta_1 - \theta_2) - \beta(\dot{\theta}_1 - \dot{\theta}_2) \tag{3}$$

In the rest of the paper, the damping in the system is ignored in the controller design because the Coulomb friction dominates the nonconservative forces. If the velocity of the inertia J_1 is constrained not to change sign during the maneuver, the friction force $f_c \operatorname{sign}(\dot{\theta}_1)$ becomes f_c and the resulting equations of motion are linear.

The discrete-time state space representation of the resulting linear system is

$$x(k+1) = Ax(k) + B(u(k) - f_c) \tag{4}$$

where the state vector is $x(k) = [\theta_1 \ \ \theta_2 \ \ \dot{\theta}_1 \ \ \dot{\theta}_2]^T$. The initial and final states are

$$x(1) = \begin{bmatrix} 0 \\ 0 \\ 0 \\ 0 \end{bmatrix} \quad \text{and} \quad x(N+1) = \begin{bmatrix} \theta_f \\ \theta_f \\ 0 \\ 0 \end{bmatrix} \tag{5}$$

where N is the number of samples in the discretized maneuver time $[0 \ \ t_f]$.

Since the system is linear, linear programming can be exploited to solve for the optimal control profile, which minimizes the maneuver time t_f subject to the constraint, so that the velocity of the inertia J_1 does not change sign.

2.1 System Subject to Friction. The state vector at the final time can be computed as a function of the initial conditions and the control history, resulting in the equation

$$x(N+1) = A^N x(1) + \sum_{k=1}^{N} A^{N-k} B u(k) - \sum_{k=1}^{N} A^{N-k} B f_c \tag{6}$$

which can be rewritten as

$$x(N+1) - A^N x(1) + \sum_{k=1}^{N} A^{N-k} B f_c = [A^{N-1}B \ \ A^{N-2}B \ \ \ldots \ \ B]\begin{bmatrix} u(1) \\ u(2) \\ \vdots \\ u(N) \end{bmatrix} \tag{7}$$

In order to satisfy the positive velocity assumption, inequality constraints that guarantee positive velocity have to be included in the LP problem. Since the velocity of the actuated disk is of interest, the output equation is

$$\dot{\theta}(k) = \underbrace{[0 \quad 0 \quad 1 \quad 0]}_{C} x(k) \tag{8}$$

These constraints must be true at every time index k. Therefore, a relationship between the output at any time k and all previous input needs to be determined. The constraint for the velocity of the inertia J_1 is

$$\dot{\theta}_1(k) = CA^N x(1) + \sum_{k=1}^{N} CA^{N-k} B u(k) - \sum_{k=1}^{N} CA^{N-k} B f_c \geq \epsilon \tag{9}$$

where ϵ is a small positive number. Equation (10) represents the velocity constraints at each time index k

$$-\begin{bmatrix} 1 & 0 & \dots & 0 & 0 \\ CB & 0 & \dots & 0 & 0 \\ CAB & CB & \dots & 0 & 0 \\ \vdots & \vdots & & \vdots & \vdots \\ CA^{N-2}B & CA^{N-2}B & \dots & CB & 0 \end{bmatrix} \begin{bmatrix} u(1) \\ u(2) \\ u(3) \\ \vdots \\ u(N) \end{bmatrix} \leq \begin{bmatrix} -f_s - \epsilon \\ CAx(1) - CBf_c - \epsilon \\ CA^2x(1) - CABf_c - CBf_c - \epsilon \\ \vdots \\ CA^{N-1}x(1) - \sum_{i=1}^{N-1} CA^{N-1-i} B f_c - \epsilon \end{bmatrix} \tag{10}$$

The first entry in the inequality constraints states that the first input must be larger than static friction to initiate motion.

The requirement that the sign of the velocity of the inertia J_1 not change sign prompts us to constrain the control profile to only include positive pulses. Systems without dissipative forces require negative pulses to bring them to rest. Since, the system being considered includes frictional forces, one can conceive of control profiles, which only include positive pulses with the knowledge that the frictional forces will dissipate the kinetic energy of the system and bring it to rest. Based on this assumption, the LP bounds on the inputs are given as

$$0 \leq u(k) \leq U_{\max} \quad \text{for } k = 1,2,\dots,N \tag{11}$$

Equations (7), (10), and (11) constitute the LP problem, which is not used to minimize a specific cost per se; rather, it is used to find a feasible input sequence that satisfies the constraints.

To obtain a minimum time solution subject to the aforementioned constraints, a bisection algorithm is used to iteratively solve for feasible control profiles, which satisfies the constraints (Eqs. (7), (10), and (11)) for a specified maneuver time t_f. The bisection algorithm determines the smallest t_f and is illustrated in Fig. 2.

2.2 LP Desensitized Control. The presumption of controller design techniques is the exact knowledge of the parameters of the system. When implementing a controller, the uncertainty in the system parameters can result in undesirable performance, which, in the case of the two-mass harmonic oscillator, uncertainties in the spring stiffness results in residual vibration at the end of the maneuver.

It is desirable to obtain a control profile that is insensitive to errors in system parameter estimates. Liu and Singh [19] presented a technique that used the concept of sensitivity states, which are defined as the derivative of the states with respect to the uncertain parameters. By forcing the sensitivity states to zero at the end of the maneuver, robustness to modeling errors is achieved. For the system under study, the uncertain parameter is taken to be the system stiffness k.

The sensitivity states are defined as

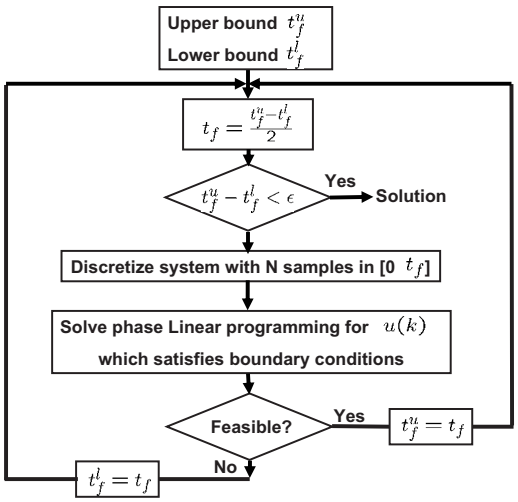

Fig. 2 Bisection algorithm

$$\theta_{1s} = \frac{d\theta_1}{dk}, \quad \theta_{2s} = \frac{d\theta_2}{dk} \tag{12}$$

The states θ_1 and θ_2 are functions of the parameter k and their sensitivities are required to be zero at the final time t_f. Differentiating the equations of motion (Eq. (1)) with respect to k results in

$$\begin{aligned} J_1\ddot{\theta}_{1s} + \theta_1 + k\theta_{1s} - \theta_2 - k\theta_{2s} = 0 \\ J_2\ddot{\theta}_{2s} - \theta_1 - k\theta_{1s} + \theta_2 + k\theta_{2s} = 0 \end{aligned} \tag{13}$$

Rewriting Eq. (13) in a matrix form, we have

$$\begin{bmatrix} \ddot{\theta}_{1s} \\ \ddot{\theta}_{2s} \end{bmatrix} = -\begin{bmatrix} 1/J_1 & -1/J_1 & k/J_1 & -k/J_1 \\ -1/J_2 & 1/J_2 & -k/J_2 & k/J_2 \end{bmatrix} \begin{bmatrix} \theta_1 \\ \theta_2 \\ \theta_{1s} \\ \theta_{2s} \end{bmatrix} \tag{14}$$

which reveals the relationship between the two equations. Using the elementary row operation $\mathcal{R}_1/J_2 + \mathcal{R}_2/J_1$, Eq. (14) can be rewritten as

$$\begin{bmatrix} \ddot{\theta}_{1s} \\ \ddot{\theta}_{1s}/J_2 + \ddot{\theta}_{2s}/J_1 \end{bmatrix} = -\begin{bmatrix} 1/J_1 & -1/J_1 & k/J_1 & -k/J_1 \\ 0 & 0 & 0 & 0 \end{bmatrix} \begin{bmatrix} \theta_1 \\ \theta_2 \\ \theta_{1s} \\ \theta_{2s} \end{bmatrix} \tag{15}$$

which shows that the two sensitivity equations of motion are not independent and only one is necessary to capture the dynamics of the two. From Eq. (15), the relationship between the sensitivity states is found to be

$$\ddot{\theta}_{1s} = -\frac{J_2}{J_1}\ddot{\theta}_{2s} \tag{16}$$

The boundary conditions of the sensitivity states at the initial time are

$$\theta_{1s}(0) = \theta_{2s}(0) = \dot{\theta}_{1s}(0) = \dot{\theta}_{2s}(0) = 0$$

Integrating Eq. (16) twice and using the boundary conditions of the sensitivity states, the relationship between θ_{1s} and θ_{2s} is

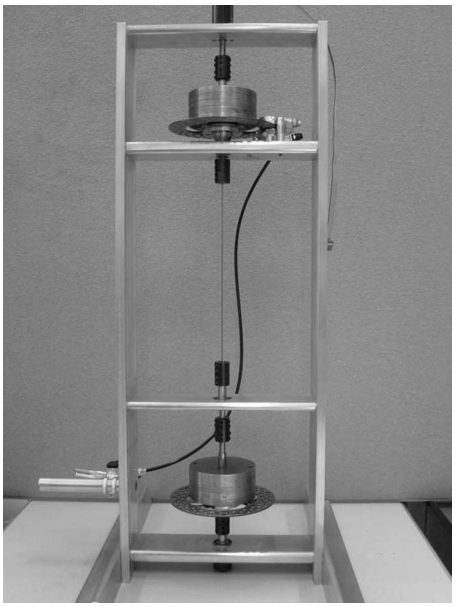

Fig. 3 Two-mass spring harmonic oscillator subject to friction

$$\theta_{1s}(t) = -\frac{J_2}{J_1}\theta_{2s}(t) \tag{17}$$

Combining Eq. (17) and the first equation in Eq. (13) results in the sensitivity state equation

$$\ddot{\theta}_{2s} = \frac{1}{J_2}(\theta_1 - \theta_2) - \left(\frac{k}{J_1} + \frac{k}{J_2}\right)\theta_{2s} \tag{18}$$

Augmenting the equations of motion with the state sensitivity equation results in the new equations of motion in the continuous time domain

$$\begin{bmatrix} J_1 & 0 & 0 \\ 0 & J_2 & 0 \\ 0 & 0 & 1 \end{bmatrix}\begin{bmatrix} \ddot{\theta}_1 \\ \ddot{\theta}_2 \\ \ddot{\theta}_{1s} \end{bmatrix} + \begin{bmatrix} k & -k & 0 \\ -k & k & 0 \\ -\frac{1}{J_2} & -\frac{1}{J_2} & \frac{k}{J_1}+\frac{k}{J_2} \end{bmatrix}\begin{bmatrix} \theta_1 \\ \theta_2 \\ \theta_{1s} \end{bmatrix} = \begin{bmatrix} 1 \\ 0 \\ 0 \end{bmatrix}(u - f_c) \tag{19}$$

The discrete-time state space equations can be derived from Eq. (19) and used in the same LP formulation as in Sec. 2.1.

3 Experimental Setup and Results

To illustrate the performance of the proposed control technique, an experimental setup to emulate the dynamics of the floating oscillator is designed. Section 3.1 describes the experimental setup. This is followed by the presentation and analysis of the experimental results in Sec. 3.2.

3.1 Hardware, Software, and System Identification. An experimental testbed of a two-mass harmonic oscillator subject to friction is built to evaluate the controllers proposed in this paper. Figure 3 illustrates the experiment, which includes two inertias connected by a torsional spring.

The motor that is used to drive the inertia at the top of the experiment is the *MicroMo 4490 024B* model, with a recommended no load torque operation of 0.192 N m. The nominal torque that is used throughout this work is 3.5×10^{-3} N m. This was calculated for an inertial load of 2.75×10^{-4} kg m^2 and a max velocity of approximately 2 rev/s reached in 1 s (i.e., acceleration=2 rad/s^2). This torque value is used as a reference point for nominal torque values and is not a restrictive bound. A brushless type motor is chosen over its iron-core counterpart due to friction considerations. The iron-core motors typically use a gear box to achieve similar torque values, and backlash in the gears can complicate the testing process.

Table 1 Experimental parameters of a two-mass harmonic oscillator

System variable	Estimated value
$\hat{J}_1$ (N m s^2)	0.00214
$\hat{J}_2$ (N m s^2)	0.01129
$\hat{k}$ (N m/rad)	1.585
$\hat{f}_c$ (N m)	0.1190
$\hat{f}_s$ (N m)	0.25

The amplifier that is used to drive the motor is a *MicroMo MVP2001 A01 Driver Electronics* (*MVP*). The motor is commanded via serial commands to the MVP. The dynamics of the electronics of motor (MVP, magnetic fields, etc.) are assumed to be negligible. An identification of the amplifier and motor reveals that a model of a rigid body system subject to damping can be used to reasonably fit the experimental data. Therefore, the inertia and damping of the motor can be lumped with that of the rotating mass. Two *US Digital E6S* series encoders with 2048 cycles per revolution quadrature (4 pulses per cycle) output are used to query the position of both masses. A *Formula Evoluzione 9.5 Disk Brake Set* is mounted on the inertias and applies the desired friction force.

LABVIEW[2] is used as the real time data processing software for all the experiments [20,21]. MATLAB[3] is used for all pre- and post-processings (i.e., trajectory construction, optimizations, etc.) of data and for processing the results [22].

Through extensive system identification of the apparatus, the system parameters are estimated and are shown in Table 1.

3.2 Experimental Results. The LP solutions for the nonrobust and robust approaches are shown in Figs. 4(*a*) and 4(*b*). The sampling time used in the LP was 0.005 s since the sampling time in LABVIEW is limited to 0.005 s. The desired final position is $x_f = 1$ rad and the maximum input value $U_{\max}$ is taken to be 3.8×10^{-3} N, which corresponds to 0.60 V. It should be noted that the proposed technique is essentially for small displacements. The final displacement of 1 rad has been selected for illustrative purposes only.

The gradually decreasing regions in Figs. 4(*a*) and 4(*b*), are where the simulation show the first mass as being stuck. In order to satisfy the positive velocity constraints, the LP solution provides a spring compensation force to ensure that the velocity of the first mass does not change sign. If the coefficient of stiffness is incorrectly estimated, it is possible that the constraint that the velocity does not change sign can be violated. This is due to the fact that the applied control is applied to compensate for the spring force acting on the mass, when the mass is stationary. By reducing the potential energy resident in the spring by using the state sensitivity with respect to the spring stiffness in the design, one can alleviate the effects of errors in estimated spring stiffness.

Twenty-five experiments were performed with the resulting input profiles. The solid lines in Fig. 5 illustrate the extreme experimental results obtained using the nonrobust input profile shown in Fig. 4(*a*) for the first (Fig. 5(*a*)) and second (Fig. 5(*b*)) masses, respectively. The dashed line corresponds to the experimental result with the smallest steady-state error. The steady-state values range from $0.9\ \text{rad} \le x_d \le 1.2\ \text{rad}$, which is approximately -10–20% from the desired value. The extreme results shown for the first and second masses are for the same experiments (i.e., the

[2]LABVIEW is a registered trademark of National Instruments, Inc.
[3]MATLAB is a registered trademark of The MathWorks, Inc., Natick, MA.

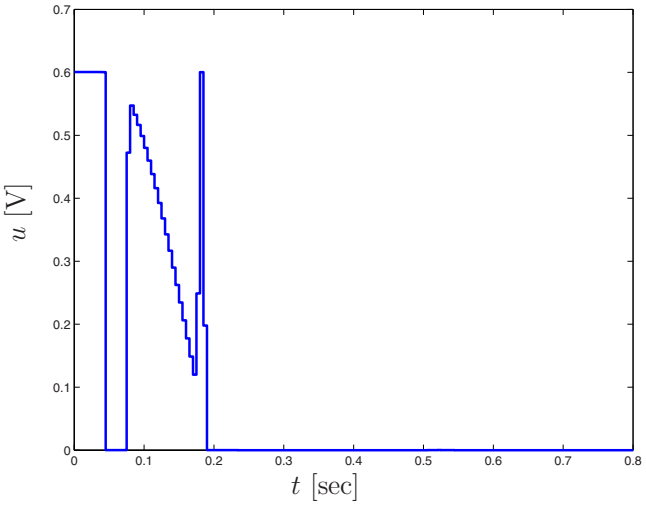

(*a*) Non-robust input profile

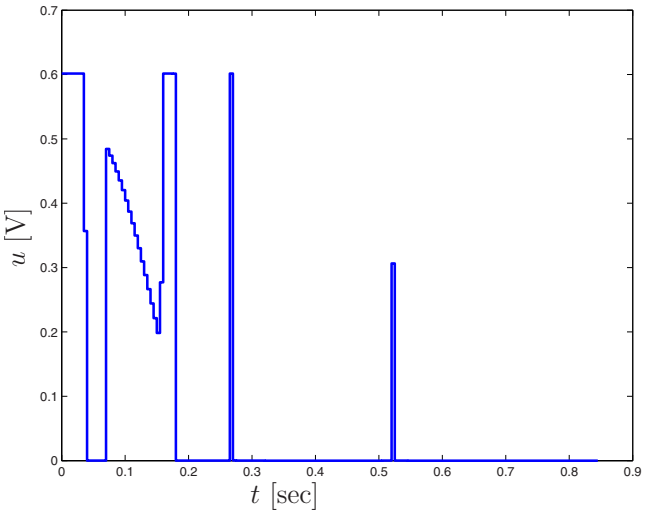

(*b*) Robust input profile

Fig. 4 LP solutions for the nonrobust and robust controllers

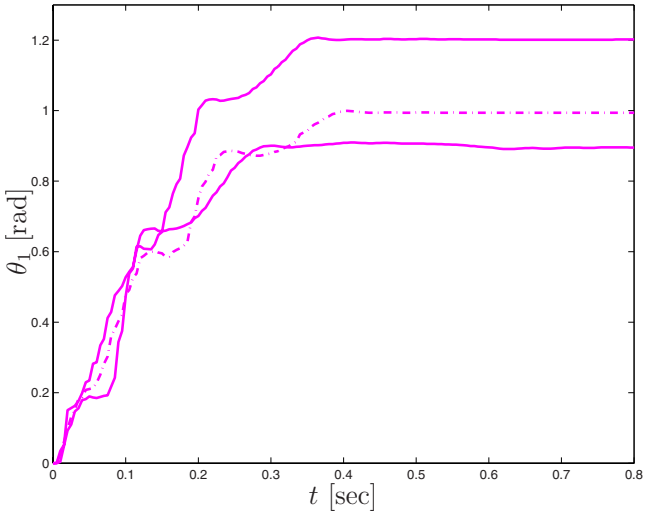

(*a*) First mass Responses

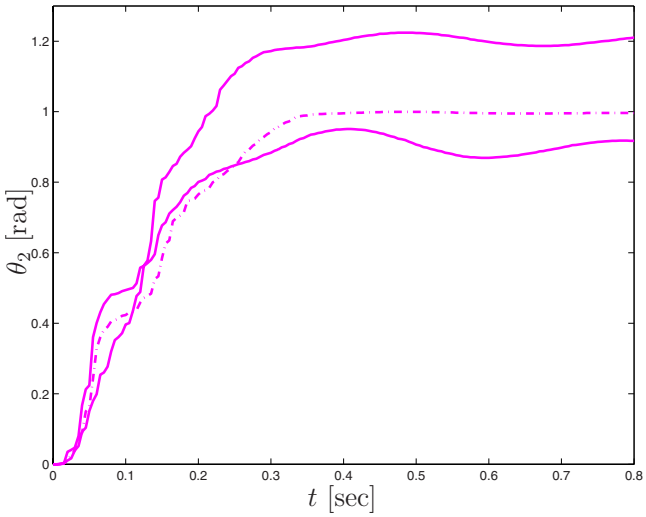

(*b*) Second mass Responses

Fig. 5 Bounds on the response of the two-mass system (nonrobust input)

maximum steady-state errors for the first and second masses come from the same experiment). It should be noted that for larger steady-state errors for the first mass, which get stuck before the second mass comes to rest, corresponds to larger vibration for the second mass. This indicates a strong coupling between the estimate of friction and the residual vibration of the system.

The extreme cases also result in large residual vibrations, which are due to deviations in friction estimates. The spring loaded friction pad results in time varying frictional force due to the wear of the pad and a state dependent variation in the frictional force due to slight warpage in the disk, which results in different normal forces acting on the inertia. In general this type of nonlinearity is inherent to experimentation. This must be ignored, however, to simplify analysis and controller design. Despite the simplifications made, an understanding of the "true" system is necessary to explain the experimental results.

Throughout the 25 experiments, the first mass trajectory occasionally has a change in sign of the velocity. This is mainly attributed to stiffness and friction uncertainties. In the LP development, the friction is assumed to be constant and known, as seen in Eq. (6). However, the velocity sign change is minor enough that the LP solution is still effective. It is important to point out that the effectiveness of the controller, despite the assumptions made, is reasonable for the open loop system. The position of the second mass also shows that the vibration is canceled by the end of the maneuver.

Figure 6 shows the worst and best experimental results for the robust case. Again, the assessment of the performance is based on the steady-state error, which is directly correlated with residual vibration of the second mass. Just as in the nonrobust case, the plots for the maximum and minimum steady-state errors for both the first and second masses come from the same experiment.

Comparing Figs. 6 and 5, it is seen that the worst case scenarios have improved for the robust case by resulting in less oscillation for the duration of the maneuver. There is also less variation across the experiments. This is most clearly seen in the first 0.2 s of the experimental results. The nonrobust results have more overlaps between the worst case results, as opposed to the robust case where the trajectories are relatively close to each other. Also, it is seen that the amplitude of oscillation for the worst cases are less than the nonrobust counterparts.

Another significant improvement in the robust result is that overall, the steady-state error has decreased. It has decreased to about $\pm 10\%$ from the previous ± 10–20%. The robust controller was designed to be insensitive to variation in the spring constant k, which is related to the natural frequency of the system. Therefore, it is expected that vibration near the reference point will be

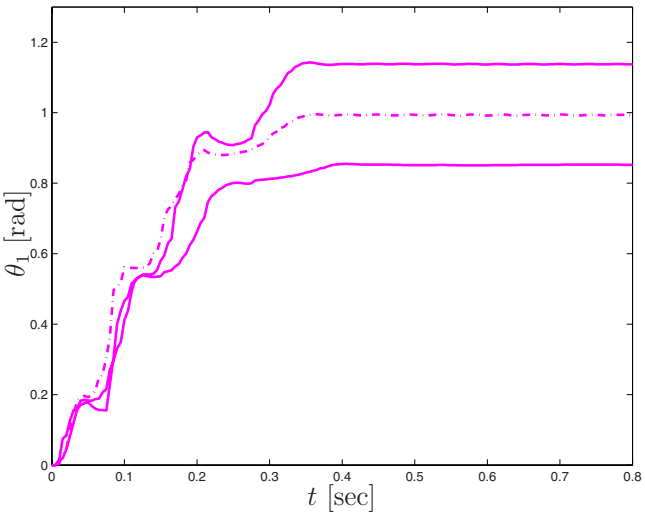

(*a*) First mass Responses

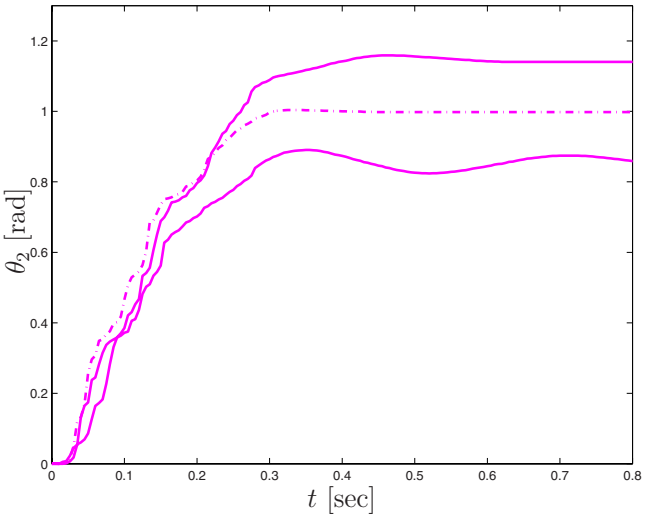

(*b*) Second mass Responses

Fig. 6 Bounds on the response of the two-mass system (robust input)

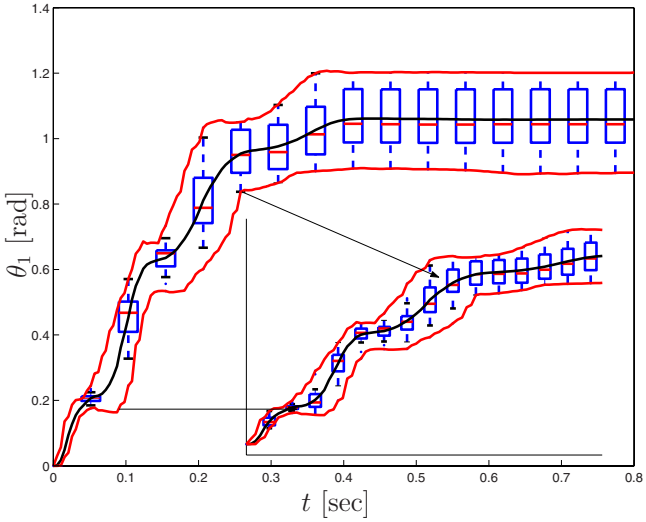

(*a*) First mass Responses

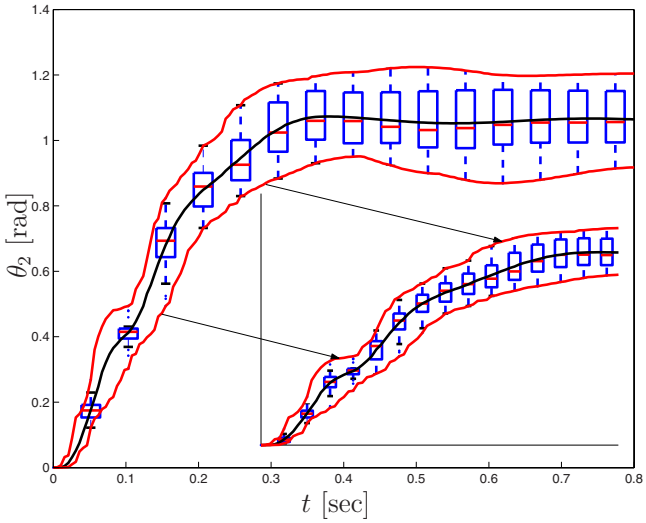

(*b*) Second mass Responses

Fig. 7 Box plot time response of the two-mass system (nonrobust input)

less than that of the nonrobust formulation, as is the case. This decreased band of oscillation decreases the range for the first mass to get stuck in, at the end of the maneuver, thus decreasing the steady-state error.

In order to display the repeatability of the experiment, the distribution of the 25 experiments are displayed with a "Box-and-Whisker" distribution plot, mainly used in descriptive statistical analysis [23]. The box-and-whisker plot is represented by five numbers in the sorted data set: the minimum, first quartile, median, third quartile, and maximum values. It is a convenient way of showing the deviation of the entire data set from these points. The outlying data points are not considered when determining the minimum and maximum, but they are used to determine the quartiles and are shown as single dots in the plot that are placed beyond the whiskers.

Figure 7 illustrates the box plot distribution for the first and second masses across all experiments for the nonrobust case. The middle trajectory represents the mean value of all experiments for each time kT. The bounding curves are the maximum and minimum of all experiments for each time kT. None of these curves represent an actual experimental trajectory. Each box plot represents the distribution of all experiments for that particular time. For the initial motion of the masses, a finer distribution is shown in an inset to highlight the performance in that region.

The general trend in the range of the distribution is that it increases as the position and velocity increase. It is expected that the response distribution will be larger as the mass displacement increases, since this spans a larger contact region over which the friction can vary.

The improvement in the robust solution is further emphasized in the box-and-whisker evolution plot seen in Fig. 8. The evolution of the positions generally have less variation across experiments. The same trends of increased variation as a function of time are illustrated, as shown in Fig. 7, for the nonrobust formulation.

A further comparison between the robust and nonrobust solutions is seen in Figs. 9 and 10. The maximum and mean magnitudes of the absolute value of the torsional spring force across all 25 experiments are plotted for both the nonrobust and robust controllers, respectively. It is seen that the maximum torsional spring force for the robust design is approximately 20% lower than for the nonrobust case. Furthermore, the spring force has been reduced throughout the entire maneuver. Since, the spring force is the reason for the change in the sign of the velocity of the first

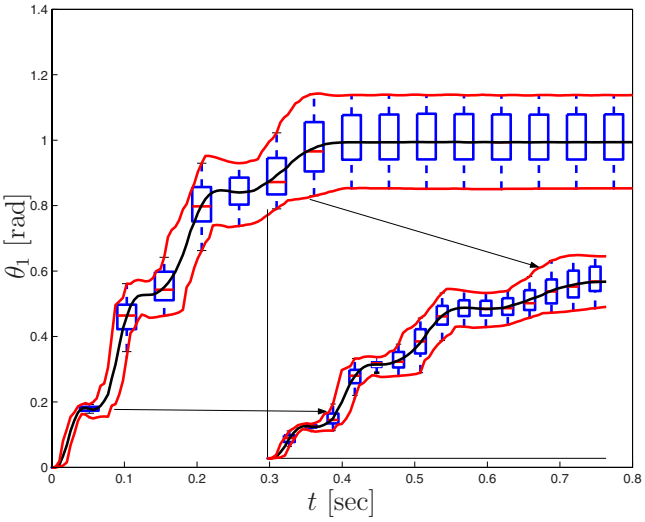

(*a*) First mass Responses

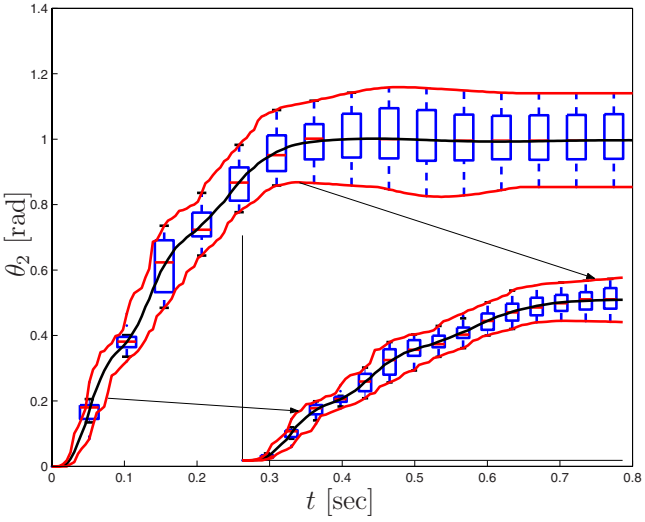

(*b*) Second mass Responses

Fig. 8 Box plot time response of the two-mass system (robust input)

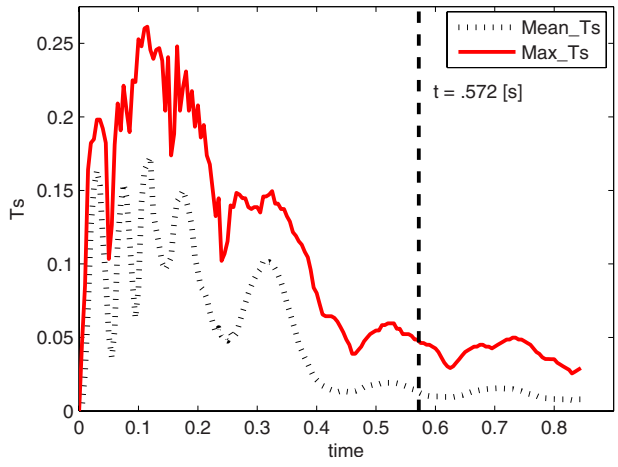

Fig. 9 Maximum and mean spring torques over 25 experiments (nonrobust control)

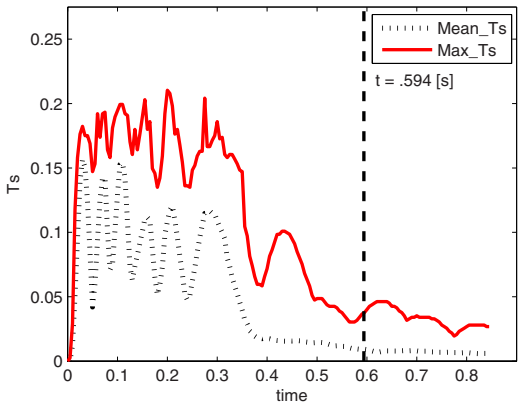

Fig. 10 Maximum and mean spring torques over 25 experiments (robust control)

mass, reducing the spring force corresponds to reducing the probability that the spring force will dominate the inertial and input forces. This consequently will result in smaller residual error in the presence of uncertainties in the spring stiffness.

The vertical dashed line shown in Figs. 9 and 10 correspond to the times where the systems were designed to have completed their maneuvers. Comparing the mean torsional spring displacement magnitude for the nonrobust and robust controller designs show that there is residual energy in the system after the designed final time $t=0.572$ s in the nonrobust approach. The oscillations indicate a transfer of energy of the masses from potential to kinetic. The oscillations of the robust approach are reduced as compared with the nonrobust approach, showing a reduction in residual vibration in the system at the end of the maneuver.

4 Conclusions

A linear programming technique based on the work of Kim and Singh [18] was implemented on a two-mass harmonic oscillator subject to friction for the robust and nonrobust cases. This technique only requires the user to select the sampling time. The LP approach automatically selects input sequence values at every sample in the interval. Reducing the final time forces the LP result to be pulses except for a short duration where the control input cancels the continuously varying spring force. The robust solution illustrates a reduction in the steady-state error and residual vibration compared with the nonrobust LP approach.

Acknowledgment

The authors would like to thank *Formula* (http://www.formula-brake.it) for their kind donation of the hydraulic disk brake set used to provide a user selected fiction force on the rotary inertia.

References

[1] Vanderplaats, G. N., 1984, *Numerical Optimization Techniques for Engineering Design With Applications, McGraw-Hill Series in Mechanical Engineering*, McGraw-Hill, New York.
[2] Driessen, B. J., 2000, "On-Off Minimum-Time Control With Limited Fuel Usage: Near Global Optima Via Linear Programming," *Proceedings of the American Control Conference, ACC*, pp. 3875–3877.
[3] Bashein, G., 1971, "A Simplex Algorithm for On-Line Computation of Time Optimal Controls," IEEE Trans. Autom. Control, **16**, pp. 479–482.
[4] Kim, M., and Engell, S., 1994, "Speed-Up of Linear Programming for Time-Optimal Control," *Proceedings of the American Control Conference, ACC*.
[5] Singh, T., and Vadali, S. R., 1994, "Robust Time-Optimal Control: A Frequency Domain Approach," J. Guid. Control Dyn., **17**, pp. 346–353.
[6] Singhose, W., Singh, T., and Seering, W., 1999, "On-Off Control With Specified Fuel Usage," ASME J. Dyn. Syst., Meas., Control, **121**, pp. 206–212.
[7] Yang, S., and Tomizuka, M., 1988, "Adaptive Pulse Width Control for Precise Positioning Under the Influence of Stiction and Coulomb Friction," ASME J. Dyn. Syst., Meas., Control, **110**, pp. 221–227.
[8] van de Wijdeven, J., and Singh, T., 2003, "Adaptive Pulse Amplitude Pulse Width Control of Systems Subject to Coulomb and Viscous Friction," *Pro-*

ceedings of the American Control Conference, Denver, CO.
[9] Kim, B. J., and Chung, W. K., 2002, "Motion Control of Precision Positiong Systems Using Adaptive Compensation," *Proceedings of the American Control Conference*, pp. 4589–4594.
[10] Altpeter, F., Myszkorowski, P., Kocher, M., and Longchamp, R., 1997, "Friction Compensation: PID Synthesis and State Control," *Proceedings of the European Control Conference*, p. TH-M-I1.
[11] Wu, R.-H., and Tung, P.-C., 2004, "Fast Pointing Control for Systems With Stick-Slip Function," ASME J. Dyn. Syst., Meas., Control, **126**, pp. 614–626.
[12] Kwatny, H., Teolis, C., and Mattice, M., 2002, "Variable Structure Control of Systems With Uncertain Nonlinear Friction," Automatica, **38**, pp. 1251–1256.
[13] Armstrong, B., Neevel, D., and Kusik, T., 2001, "New Results in NPID Control: Tracking, Integral Control, Friction Compensation and Experimental Results," IEEE Trans. Control Syst. Technol., **9**, pp. 399–406.
[14] Rathbun, D. B., Berg, M. C., and Buffinton, K. W., 2003, "Pulse Width Control for Precise Positioning of Structurally Flexible Systems Subject to Stiction and Coulomb Friction," ASME J. Dyn. Syst., Meas., Control, **126**, pp. 131-138.
[15] Hamamoto, K., Fukuda, T., and Sugie, T., 2003, "Iterative Feedback Tuning of Controllers for a Two-Mass-Spring System With Friction," Control Eng. Pract., **11**, pp. 1061–1068.
[16] Driessen, B., and Sadegh, N., 2001, "Minimum-Time Control of Systems With Coulomb Friction: Near Global Optima Via Mixed Integer Linear Progamming," Opt. Control Appl. Methods, **22**, pp. 51–62.
[17] Lawrence, J., Singhose, W., and Hekeman, K., 2005, "Friction-Compensating Input Shaping for Vibration Reduction," ASME J. Vibr. Acoust., **127**, pp. 307–314.
[18] Kim, J. J., and Singh, T., 2004, "Desensitized Control of Vibratory Systems With Friction: Linear Programming Approach," Opt. Control Appl. Methods, **25**, pp. 165–180.
[19] Liu, S.-W., and Singh, T., 1997, "Robust Time-Optimal Control of Flexible Structures With Parametric Uncertainty," ASME J. Dyn. Syst., Meas., Control, **119**, pp. 743–748.
[20] Travis, J., 2002, *LABVIEW for Everyone, National Instruments Virtual Instrumentation Series*, 2nd ed., Prentice Hall, Upper Saddle River, NJ.
[21] Bishop, R. H., 2001, *Learning With LABVIEW*, 6th ed., Prentice Hall, Upper Saddle River, NJ.
[22] The Math Works, Inc., 2001, "Optimization Toolbox For Use With MATLAB Version 2.1.1," Release 12.1, online only.
[23] Larson, R., and Farber, B., 2003, *Elementary Statistics: Picturing the World*, 2nd ed., Prentice Hall, Upper Saddle River, NJ.